NASA TECHNICAL MEMORANDUM

NASA TM X-73988

NASA TM X-73988

EFFECT OF LOW VELOCITY IMPACT DAMAGE ON THE COMPRESSIVE STRENGTH OF GRAPHITE/EPOXY HAT-STIFFENED PANELS

by

Marvin D. Rhodes, Jerry G. Williams, and James H. Starnes, Jr.

December 10, 1976

National Aeronautics and Space Administration

Langley Research Center
Hampton, Virginia 23665

1. Report No.	2. Government Accession No.	3. Recipient's Catalog No.
NASA TM X-73988		

4. Title and Subtitle	5. Report Date
EFFECT OF LOW VELOCITY IMPACT DAMAGE ON THE COMPRESSIVE STRENGTH OF GRAPHITE/EPOXY HAT-STIFFENED PANELS	December 1976
	6. Performing Organization Code
7. Author(s)	8. Performing Organization Report No.
Marvin D. Rhodes, Jerry G. Williams, and James H. Starnes, Jr.	
	10. Work Unit No.
9. Performing Organization Name and Address	
NASA Langley Research Center Hampton, VA 23665	11. Contract or Grant No.
	13. Type of Report and Period Covered
12. Sponsoring Agency Name and Address	Technical Memorandum
National Aeronautics and Space Administration Washington, D.C. 20546	14. Sponsoring Agency Code

15. Supplementary Notes

16. Abstract

An experimental investigation was conducted to determine the effect of low velocity impact damage on the compressive strength of graphite/epoxy hat stiffened panels. Fourteen panels, representative of minimum-mass designs for two compression load levels (0.53 MN/m and 1.58 MN/m), were tested. Eight panels were damaged by impact and the effect on compressive strength was evaluated by comparing the results with data for undamaged panels. The impact tests consisted of firing 1.27 cm diameter aluminum projectiles normal to the plane of the panel at a velocity of approximately 55 m/sec to simulate impact from runway debris.

The results of this investigation indicate that impact damage in the panels designed for 0.53 MN/m was contained locally and the damaged panels were capable of carrying the design load. The panels designed for 1.58 MN/m, however, failed between 50 and 58 percent of the design load due to impact damage in the high axial stiffness region. The extent of damage in the high axial stiffness region of both panel designs increased with the magnitude of applied axial load. However, the existence of and not necessarily the extent of, damage in this region was the most significant factor in reducing panel strength. Limited damage that was not visually detectable reduced ultimate strength as much as extensive visible damage.

17. Key Words (Suggested by Author(s))	18. Distribution Statement
Composite structure Impact damage	Unclassified - Unlimited

19. Security Classif. (of this report)	20. Security Classif. (of this page)	21. No. of Pages	22. Price*
Unclassified	Unclassified	29	$3.75

*For sale by the National Technical Information Service, Springfield, Virginia 22161

EFFECT OF LOW VELOCITY IMPACT DAMAGE ON THE COMPRESSIVE STRENGTH OF GRAPHITE/EPOXY HAT-STIFFENED PANELS

by

Marvin D. Rhodes, Jerry G. Williams, and James H. Starnes, Jr.

CONTENTS

INTRODUCTION 1
DESIGN AND FABRICATION OF TEST SPECIMENS 2
Specimen Design 3
Design A 3
Design B 3
Specimen Fabrication. 3
APPARATUS 4
TESTS 5
Control Tests 5
Undamaged panels 5
Panel with a cutout. 5
Impact Damage Tests 5
RESULTS AND DISCUSSION 6
Control Tests 6
Undamaged panels 6
Panel with a cutout. 6
Impact Damaged Panels 8
Impact damage in the high axial stiffness region 8
Low axial strain at impact. 8
High axial strain at impact 9
Impact damage characterization. 10
Impact damage in the low axial stiffness region. 11
CONCLUDING REMARKS 12
REFERENCES 14
TABLES 15
FIGURES. 17

EFFECT OF LOW-VELOCITY IMPACT DAMAGE ON THE COMPRESSIVE STRENGTH OF GRAPHITE/EPOXY HAT-STIFFENED PANELS

By

Marvin D. Rhodes, Jerry G. Williams

and

James H. Starnes, Jr.

INTRODUCTION

The most efficient hat-stiffened graphite/epoxy compression panels have been shown to be approximately 50 percent lighter than the most efficient aluminum compression panels (Refs. 1 and 2). This mass reduction makes graphite/epoxy panels attractive candidates for aircraft applications, but before they can be used in commercial service certain operational hazards must be considered. For example, aircraft can be subjected to impact damage from runway debris and the effects of such damage must be established. Low velocity impact damage has been shown to cause significant reductions in the load carrying capability of some thin honeycomb stabilized graphite/epoxy laminates (Refs. 3 and 4). Little work, however, has been done to assess the effect of impact on stiffened compression panels.

This paper presents the results of an exploratory test program to determine the effect of low velocity impact damage on minimum mass hat-stiffened panels. The panels were designed for two different compression loads [0.53 MN/m (3000 lbf/in) and 1.58 MN/m (9000 lbf/in)] with buckling as the primary design constraint. The test results presented include data for undamaged panels, data for a panel with a 1.27 cm diameter cutout and, data for panels subjected to impact damage. The undamaged panels were used to verify the design and establish critical strain levels for compression loading. The panel with the 1.27 cm diameter cutout, which simulated local damage, provided comparative data for a panel with a well defined flaw. The impact damaged panels were used to determine the effect of this type of damage for a range of applied strain. These panels were subjected to impact damage while under load to evaluate the effect of applied strain on local damage, and some were subsequently loaded to evaluate residual strength.

DESIGN AND FABRICATION OF TEST SPECIMENS

Hat-stiffened panels with minimum mass proportions of two different designs (designated designs A and B) were tested in this investigation. Design A was critical in buckling at a load of 0.53 MN/m (3000 lbf/in) which corresponds to an axial strain of 0.0034. Design B was more heavily loaded [1.58 MN/m (9000 lbf/in)] and was critical in buckling at a strain of 0.008. The basic configuration for both designs is shown schematically in sketch a.

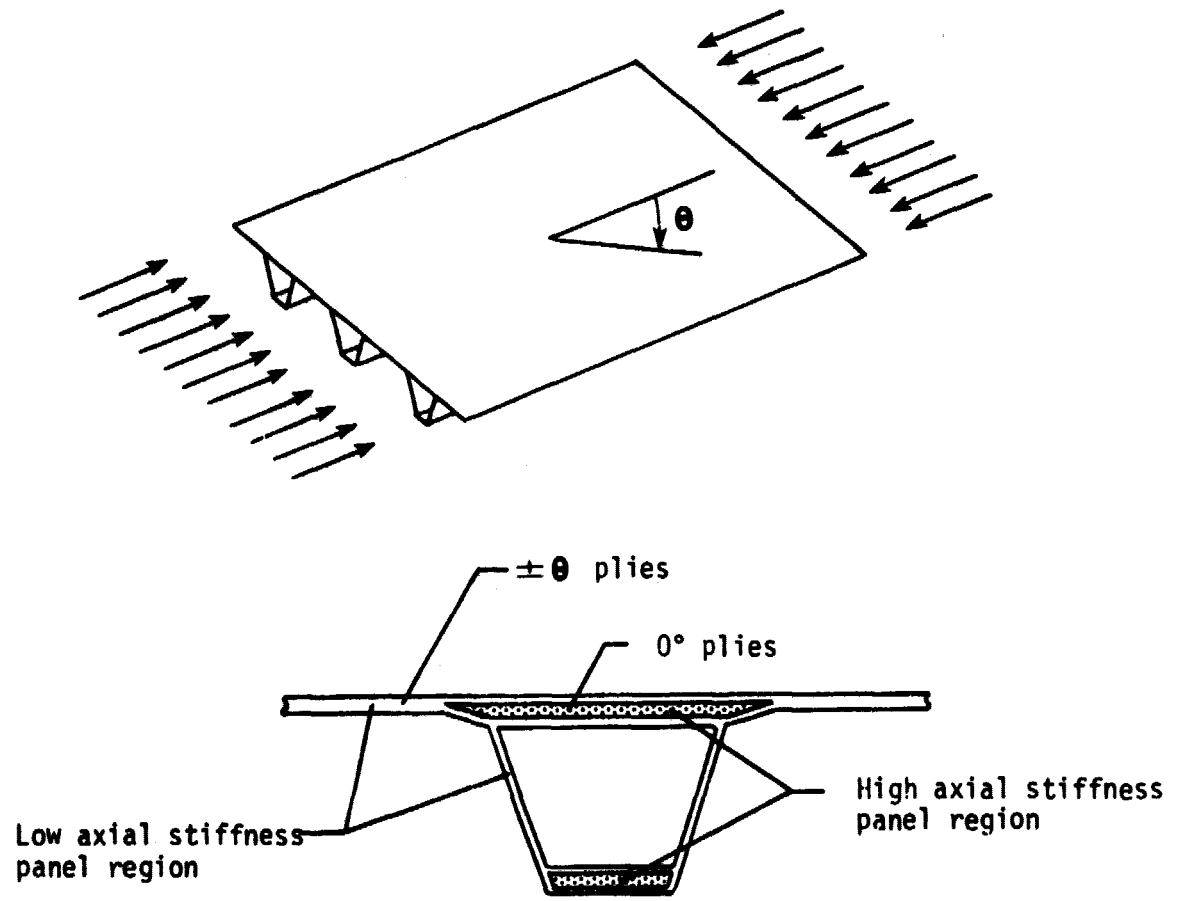

Sketch a.- Hat-stiffened panel.

Specimen Design

Panels were designed from the material properties given in Table I using a minimum-mass synthesis computer program that includes buckling and strength constraints (ref. 5). The buckling constraints accounted for simply supported wide-column Euler buckling as well as local buckling, i.e., short wavelength panel buckling of the skin, stiffener caps and webs. The bending stiffness required for wide-column Euler-buckling is primarily provided by the high axial stiffness 0° plies located in the cap of the hat and concentrated in the skin beneath the hat (Sketch a). The webs and skin between stringers consist entirely of angle plies ($\pm\theta$). The critical Euler-buckling design length for both panel types is 76.2 cm. Specimens tested in this investigation were 43.7 cm or less in length and, therefore, were only local buckling critical. Since the test panels are critical in both local and Euler buckling at the design load, the test length did not significantly affect the panel strength.

Design A.- Details of the cross-section of the panels designed to carry a load of 0.53 MN/m, are presented in figure 1(a). At this design load the panels had an imposed axial strain of 0.0034. The angle plies in the webs and skin were oriented at $\pm 52^\circ$. The final design mass per unit area was 3.56 kg/m^2 (0.73 lbm/ft^2). Both three stiffener wide and four stiffener wide panels were tested in this investigation. Test panel dimensions (panels A1-A5) are given in Table II.

Design B.- Details of the cross-section of the panels designed to carry a load of 1.58 MN/m are presented in figure 1(b). At this design load the panels had an imposed axial strain of 0.0080. The angle plies in the webs and skin were oriented at $\pm 45^\circ$. The panel design mass per unit area was 6.10 kg/m^2 (1.25 lbm/ft^2). Both two stiffener wide and three stiffener wide panels were tested in this investigation. Test panel dimensions (panels B1 - B9) are given in Table II.

Specimen Fabrication

The specimens tested in this investigation were fabricated from 7.6 cm wide preimpregnated tape of Thornel 300 graphite in Narmco 5208 epoxy resin. The resin is a 450 K ($350^\circ F$) curing system and the tape has a nominal cured thickness of 0.14 mm (.0055 in) per ply. The specimens were manufactured

using an aluminum tool which was machined with the required hat stiffener design cross-sectional dimensions. The $\pm\theta$ web and 0° hat plies were laid in the mold. Premolded trapezoidal-shaped rubber inserts were positioned in the mold and the skin plies were laid on top. The panel was covered by an aluminum caul plate and the entire assembly was bagged and cured in an autoclave. The cured specimens were then trimmed; the ends were potted in an epoxy resin and ground flat and parallel for uniform compression loading. Detail design considerations, analysis methods and manufacturing procedures are described in references 1 and 2.

APPARATUS

The test specimens were loaded in axial compression using a hydraulic test machine with a 1.33 MN capacity. Electrical resistance strain gages were used to monitor panel strains. A direct-current-differential transformer (DCDT) was used to monitor displacements normal to the surface of the panels. Strains, displacements, and load were recorded on magnetic tape and selected gages were monitored during the test on an oscilloscope. The moiré method for observing lateral displacements was used to monitor buckle patterns and delamination growth during loading. The basic instrumentation for this purpose included a high-intensity light source, a grid pattern of 20 lines per cm mounted on a transparent plastic sheet held near the specimen, and a camera to record photographically the fringe pattern at selected loads.

The equipment used to propel the impact projectile is shown schematically in figure 2. Air pressure developed in the reservoir ruptures the diaphragm. The high pressure air passes through an orifice and forces the projectile down the barrel. An electronic detector located at the muzzle of the barrel is used to measure the velocity of the projectile. The test panels were placed within 25 cm of the gun muzzle.

Several panels with impact damage were examined with an ultrasonic flaw-detector. The detector was a focused pulse-echo type high-resolution commercial instrument which used a 15 MHz piezoelectric transducer. The transducer and panels were immersed in a tank of water to provide a medium for the ultrasonic transmission and the transducer was mounted to a traversing mechanism which automatically scanned the region of interest. The scan was synchronized with an oscilloscope for purposes of recording data.

Additional information concerning this equipment and procedure can be found in reference 6.

TESTS

Control Tests

Undamaged panels.- Several undamaged panels were tested in compression to determine the critical load and strain at which local buckling occurred. Local buckling was defined using the load/strain response and strain-reversal techniques. The strain measurements were complemented by the moiré fringe method which provided visual definition of the buckled mode-shape.

Panel with a cutout.- A hat-stiffened panel with a 1.27 cm diameter circular hole was loaded in compression to evaluate the effect of a well defined damaged area on panel performance. The hole was located in the high axial stiffness region beneath the cap in the middle of the center stiffener. It was drilled using a diamond impregnated core bit. The panel was instrumented with approximately 40 strain gages and loaded to failure. Displacements normal to the surface in the center of the panel were measured with a DCDT. The moiré fringe technique was used to observe the development of the displacement field associated with deformations normal to the plane of the panel.

Impact Damage Tests

Several panels were damaged by impact in the high axial stiffness region while under compression load to evaluate the effect of load on impact initiated damage. The panels were then taken to higher loads to evaluate the effect of damage on buckling and residual strength. One panel was also damaged by impact in the low axial stiffness skin region between stiffeners. Aluminum spheres 1.27 cm in diameter were used as the impact projectile. Aluminum was chosen as the projectile material because it has about the same density as common rock materials and is therefore representative of runway debris. The projectile impacts were normal to the panel surface at a velocity of about 55 m/sec. Loading conditions and impact location for each panel tested are given in Table II.

RESULTS AND DISCUSSION

Control Tests

Undamaged Panels

Three panels of design A and four of design B were tested in the undamaged condition to evaluate panel behavior due to applied axial compressive load. The behavior of each panel for the indicated load and strain is presented in table II. The type A panels buckled near the design strain of 0.0034 and exhibited postbuckling behavior. The type B panels exhibited strength failure near the design strain of 0.0080 prior to buckling. A photograph of a typical normal displacement field as indicated by the moiré fringe pattern for each design configuration is shown in figure 3. Test panel A1 (figure 3a) has a fully developed buckle pattern at an imposed strain of 0.0036. Test panel B2 (figure 3b) is shown at an imposed axial strain of 0.0079 which is near the strain at which the panel exhibited failure. The pattern seen at the ends of the panel is the result of inplane restraints imposed by the flat-end test condition (ref. 2).

Panel with a Cutout

The panel (B5) with the 1.27 cm diameter cutout was loaded to failure in axial compression. Far-field axial strains were measured during the test by five strain gages located on a line across the panel, 6.35 cm from the cutout center. The location of those gages and the measured strains as a function of applied load are shown in figure 4. These data indicate a nearly uniform far-field axial strain distribution across the panel and a linear load-strain relationship to failure. The average of these gages is subsequently referred to as the applied strain. Panel failure occurred at an applied strain of 0.0058 (applied load of 496 kN) which is 73 percent of the 0.0080 design strain.

Several strain gages were located at points along a line across the panel passing through the cutout center to determine the variation in axial strain in the neighborhood of the cutout. These gages were closely spaced near the cutout and one gage was located on the cutout free-edge surface. The distribution of strain as determined by these gages across the right side of the panel is shown normalized by the applied strain in figure 5 for several

values of applied strain. The origin of all curves on figure 5 is indicated in the sketch on the figure and the distance y from the cutout edge has been normalized by the cutout radius. The strains are several times greater near the cutout edge than those three cutout radii away and there are steep strain-gradients near the cutout edge. Up to an applied strain of about 0.0034 the strain at the cutout edge is approximately 4.6 times greater than the far-field strain. At an applied strain of 0.0034 the strain at the cutout edge was 0.016 and then dropped suddenly to 0.012. It is suspected that a local material failure occurred in the zero degree laminae at this very high strain level. At applied strains between 0.0034 and 0.0049 the strains at the cutout edge were only 2.4 to 2.8 times as great as the far-field strains as indicated by the results shown on figure 5.

At applied strains near 0.0049 large changes in strain were recorded near the cutout and noticeable panel displacements began to develop in the vicinity of the cutout. Moiré fringe patterns representing the normal displacement-field near the cutout are shown in figure 6 for several values of applied strain. A representative moiré fringe pattern for an applied strain of 0.0048 is shown in figure 6a and a close up of the cutout region for this applied strain is shown in figure 6b. At an applied strain of approximately 0.0049 a local buckling displacement field began to develop at the cutout edge about 60° counterclockwise from the loading axis. This displacement-field was about 1.0 cm long for an applied strain of 0.0050 and is shown in figure 6c. As the applied strain was increased, the extent of the displacement-field increased to a length of about 1.8 cm for an applied strain of 0.0055 as shown in figure 6d. At an applied strain of 0.0057, the displacement-field had rotated counterclockwise to a position 90° from the loading axis (figure 6e) and extended on both sides of the cutout. This displacement field extended about 2.5 cm on the left side and about 2.4 cm on the right side of the cutout which makes the total length of this displacement field approximately equal to the width of the 0° fibers in the skin under the stiffener. The local displacement-field propagated across the panel (figure 6f) at an applied strain of 0.0058 which indicates that the local behavior precipitated panel failure.

Impact Damaged Panels

Impact Damage in the High Axial Stiffness Region

Low axial strain at impact.- Test panels A4, A5, and B6 were damaged by impact with a small axial load applied at the time of impact (see table II). A visual examination of the area where impact occurred revealed no apparent local damage. All three specimens were subsequently loaded in compression to failure. Several strain gages away from the impact region were used to monitor the applied axial strains. The average of these gages is subsequently referred to as the applied strain. The applied strain at failure for all three test panels is given in table II. Both panels A4 and A5 failed at applied strains near their design strain level (0.0034). A photograph of the moiré fringe pattern of panel A4 loaded prior to failure and a photograph of the failed panel are shown in figure 7. The moiré fringe pattern (figure 7a) is similar to that of the undamaged panel A1 (figure 3a). The dark spot in the center of the panel is the impact location where the paint has been removed for post impact inspection. Figure 7b indicates that the panel failure region is extensive and includes the impact location. The panel was inspected ultrasonically prior to failure and a photograph of the oscilloscope record for the region in the vicinity of the impact location is shown in the insert of figure 7a. The area represented by the insert is outlined on the photograph. The dark area shown in the insert indicates subsurface damage in the panel. This area is about 6.35 cm long and about as wide as the region beneath the hat which contains 0° plies. The results of tests on panels A4 and A5 were similar.

Panel B6 failed during the residual strength test at an applied strain of 0.0043 which is about 54 percent of the design value. A photograph of the moiré fringe pattern prior to failure and a photograph of the failed panel are shown in figure 8. A small circular pattern in the region of impact was observed with the moiré fringe technique indicating the presence of local damage. The development of this fringe pattern and an examination of the panel failure indicate that the impact damage precipitated the panel failure.

Two stiffener sections, typical of those of panel B6, were damaged by impact at zero applied axial strain and ultrasonically inspected. Identical

results were obtained for these two sections. A photographic record of the ultrasonic inspection is shown in the insert of figure 8a. The subsurface damage region is oval shaped and is about 2.54 cm wide by 3.81 cm long. One of the stiffeners was cross sectioned in the region of impact damage and examined microscopically. A photomicrograph of the cross section at a low level of magnification is shown in figure 9. This photomicrograph reveals delamination in the cross section with the most severe delamination occurring on the back surface of the laminate. Striations or hairline crack patterns through the thickness can also be observed. These cracks converge on the point of impact and are similar to those patterns observed for impact damaged glass panels. Both the cracking and the delamination are probably the result of stress waves generated by the projectile impact.

High axial strain at impact.- Test panels A3, B7 and B8 were damaged by impact with a high axial load applied (see table II). Panels A3 and B7 which had an applied axial strain of 0.0034 and 0.0030, respectively, had a large region of visually detectable damage in the impact area. Instrumentation monitoring applied load indicated both panels had significant load reductions at impact due to loss in panel stiffness (table II). Both were subsequently loaded to failure to determine the panel residual strength. Panel A3, which was loaded to 0.0034 and damaged by impact, was ultrasonically inspected prior to the residual strength test. An extensive region of subsurface damage was detected. A photograph of the moiré fringe pattern of the panel loaded prior to failure is shown in figure 10a where the subsurface damaged region is outlined. Even though the damage in panel A3 is extensive, it buckled at an applied strain near the design level and carried additional load after buckling similar to the undamaged panels. The panel failed in the region of the impact damage (figure 10b). Comparison of panel A3 with panels A4 and A5, all of which were designed for moderate strains, indicates that the extent of the subsurface damage did not significantly affect the strain level at which the panel failed.

Panel B7 failed during the residual strength test at an applied strain of 0.0046 which is about 58 percent of the design value. Several photographs of the moiré fringe pattern taken during the residual strength test are shown in figure 11 along with a photograph of the failed panel. The

moiré fringe pattern shows considerable lateral deformation of the panel center which may be due to impact induced delamination or skin buckling. When the panel was damaged by impact a reduction in applied load of 28.9 kN was measured. This is approximately the load which the high axial stiffness region beneath the center stiffener is calculated to carry for an imposed strain of 0.0030.

Panel B8 had an applied axial strain of 0.0040 (50 percent of design strain) and failed catastrophically on impact. The failure was similar to the ultimate failure of panel B7. After failure the panel was cross sectioned and examined with a microscope. This examination revealed considerable interior damage in the laminate near the impact location. Cracking similar to that previously discussed was also observed. The combination of applied axial load and dynamic stress waves generated by the projectile impact forms a complicated three dimensional stress field in the orthotropic laminates of these test panels. This suggests that a simple criterion may not be adequate to predict panel failure.

Impact damage characterization.- A comparison of test results for impact in the high axial stiffness region indicates both similarities and differences in the results for panels of design A and design B. The extent of local damage induced by impact increased with the magnitude of applied axial-compressive strain for both designs. The design A panels satisfied the design-strain requirements with impact damage and also exhibited post buckling behavior. The design B panels, however, failed due to impact damage at applied axial strains between 50 and 58 percent of the design strain level. The impact test results for both designs are summarized in figure 12 along with the cutout test data for comparison. Limited local impact damage that was not noticeable by visual inspection (Panel B6) reduced the ultimate strength of the design B panels as much as extensive visible localized damage (Panel B7). All three of the design B panels damaged by impact failed at lower applied strain levels than the control test panels with the 1.27 cm diameter cutout. The damaged region caused by impact, however, was larger than the controlled cutout. In all cases, the damage in the high axial stiffness region precipitated failure at an applied strain well below the design strain level.

The results of this investigation suggest that impact causes considerable ply delamination, and examination of the panel cross-section showed that the delamination occurred primarily at the interface between the 0° and 45° plies (fig. 9). The discrete layers formed by delamination may not be midplane symmetric and, therefore, exhibit anisotropic coupling effects. The boundaries of these discrete layers are highly irregular (fig. 10) and are subjected to high interlaminar normal and shear stresses. Also, delamination reduces the local cross-sectional bending stiffness and causes locally eccentric loading which introduces transverse shear forces and moments not present in the undamaged panel. These local eccentric forces and anisotropic effects cause local deformations and strain gradients to occur in the delaminated region that could be sufficient to make local geometric and material property nonlinearities important factors. Since these eccentrically loaded layers are thinner and less stiff than the undamaged laminate, they can buckle locally at a lower load than the undamaged laminate. This could cause a local load redistribution in the panel that, in turn, could cause the damage to propagate and the panel to fail. The results of this investigation suggest that highly efficient graphite/epoxy hat stiffened compression panels designed for high strain (0.0080) can exhibit serious degradation due to impact damage, however, efficient damage tolerant designs can be obtained for more moderate strains.

Impact Damage in the Low Axial Stiffness Region

To evaluate the effect of impact damage in the $\pm 45^{\circ}$ ply low axial stiffness region, panel B9 was damaged by impact in the skin region between stiffeners. The panel was loaded to an applied axial strain of 0.0040 when impact occurred (see table II). No reduction in the applied load was observed and no increase in axial strain was noted in the gage near the point of impact. Although some local fiber failure and delamination was observed, the failure did not propagate. After impact the panel was loaded to an applied strain of 0.0054 without propagation of local damage. At this load the panel was damaged in the remaining undamaged $\pm 45^{\circ}$ skin region between stiffeners (see table II). No loss in load or increase in strain near the point of impact was detected. This panel was subsequently loaded to an applied strain of 0.0062 at which a moiré pattern was observed in the end regions (see figure 13)

similar to that observed for the undamaged test panel. A local fringe pattern can be seen in the figure at each impact location.

Following this test the panel was inspected ultrasonically to evaluate the extent of the damage region. The subsurface damage region is outlined on the panel in figure 13. The two damaged regions are about the same size which indicates that the magnitude of the applied strain had no apparent effect on the extent of local damage. These results indicate that impact damage in the regions having high axial stiffness is significantly more detrimental than it is in regions of low axial stiffness.

CONCLUDING REMARKS

An exploratory investigation was conducted to determine the effect of low velocity impact damage on the compression strength of graphite/epoxy hat-stiffened panels. Fourteen panels were tested in this investigation and the results indicate that low velocity impact, typical of that which may be inflicted by runway debris, can have a significant effect on panel compression strength. Runway debris hazards were simulated in this study by 1.27 cm diameter aluminum spheres impacting at velocities around 55 m/s. Both high and low axial stiffness regions of the panel cross-sections were subjected to impact. The impacting sphere caused local damage in both regions. Damage to the low stiffness region was found to have little effect on panel strength. Impact damage to the high axial stiffness region caused panels designed for 1.58 MN/m at a strain of 0.0080 to fail catastrophically for applied axial strains above a value between 50 and 58 percent of the design level. Damage in the high axial stiffness regions of panels designed for 0.53 MN/m at a strain of 0.0034 was contained locally and these locally damaged panels were capable of carrying the design load.

The extent of local damage induced by impact in regions of high axial stiffness was found to increase with the magnitude of applied axial compression strain present at impact. The existence of and not necessarily the extent of local damage was found to be the significant factor in reducing the strength of panels designed for 1.58 MN/m. Limited local damage that was not visually detectable (but which could be identified by ultrasonic inspection) reduced the ultimate strength as much as extensive visible damage. Impact caused considerable ply delamination and the discrete layers thus formed

can exhibit anisotropic effects. Such delamination also introduces local eccentric forces in the panel that develop high normal and shear stresses at the boundary of the delaminated region, and these delaminated regions can buckle locally at reduced applied loads. These effects could contribute to local load redistribution in the panel and cause the damage to propagate.

A panel designed for 1.58 MN/m was tested to failure with a 1.27 cm diameter cutout in the region of high axial stiffness to provide comparative data for a panel with a well defined flaw. Two types of local failure were observed near the cutout. First, localized material failure occurred at the cutout boundary. Second, local buckling in the region of the cutout was observed prior to failure. The local buckling subsequently precipitated panel failure at 73 percent of the design strain level. This strength reduction was not as severe as that caused by impact damage; however, the impact studies herein caused a damaged region that was larger than the 1.27 cm diameter cutout.

The results of this exploratory investigation suggest that highly efficient graphite/epoxy hat-stiffened compression panels designed for a 0.0080 strain level can exhibit serious compressive strength degradation due to impact damage. However, efficient damage tolerant designs can be obtained for moderate strains, even for cases where regions of high axial stiffness are exposed to impact damage hazards.

REFERENCES

1. Williams, Jerry G.; and Mikulas, Martin M., Jr.: Analytical and Experimental Study of Structurally Efficient Composite Hat-Stiffened Panels Loaded in Axial Compression. AIAA Paper 75-754, Presented at ASME/AIAA/SAE 16th Structures, Structural Dynamics, and Materials Conference, May 27-29, 1975.
2. Williams, Jerry G.; and Stein, Manuel: Buckling Behavior and Structural Efficiency of Open-Section Stiffened Composite Compression Panels. Presented at AIAA/ASME/SAE 17th Structures, Structural Dynamics, and Materials Conference, May 5-7, 1976.
3. Rhodes, Marvin D.: Impact Fracture of Composite Sandwich Structures. AIAA Paper 75-748, Presented at ASME/AIAA/SAE 16th Structures, Structural Dynamics, and Materials Conference, May 27-29, 1975.
4. Mikulas, Martin M., Jr.; Bush, Harold G.; and Rhodes, Marvin D.: Current Langley Research Center Studies on Buckling and Low Velocity Impact of Composite Panels. Third Conference on Fibrous Composites in Flight Vehicle Design, Part II. NASA TM X-3377, April 1976.
5. Agarwal, B.; and Davis, R. C.: Minimum-Weight Designs for Hat-Stiffened Composite Panels Under Uniaxial Compression. NASA TN D-7779. November, 1974.
6. Platt, Robert J., Jr.; and Thurston, Lewis B., Jr.: Holographic and Ultrasonic Detection of Bond Flaws in Aluminum Panels Reinforced with Boron-Epoxy. NASA TN D-7632, July, 1974.

TABLE I.- ELASTIC MATERIAL PROPERTIES USED IN PANEL DESIGNS

Longitudinal Modulus	131 GN/m^2 (19.0×10^6 lbf/in^2)
Transverse Modulus	13.0 GN/m^2 (1.89×10^6 lbf/in^2)
Shear Modulus	6.41 GN/m^2 (0.93×10^6 lbf/in^2)
Major Poisson's Ratio	0.38
Density	1.52 g/m^3 (0.055 lbm/in^2)
Thickness	0.14 mm/ply (0.0055 in/ply)

DATE ____ SUBJECT ____ SHEET NO ____ OF ____
DATE ____ JOB NO ____

TABLE II.- TEST CONDITIONS AND RESULTS

Test			Panel			Load Conditions				Impact Test				Residual Strength		
			No.	Length (cm)	Width (cm)	ε_a	$\varepsilon_a/\varepsilon_D$	Load (kN)	Response	Velocity (m/s)	Location	Load After Impact(kN)	Subsurface Damage Size *	ε_a	$\varepsilon_a/\varepsilon_D$	Load(kN)
Control Panel Tests	Undamaged Panels	Design A $\varepsilon_D = 0.0034$	A1	40.4	17.8	0.0032	.94	100	Buckled							
			A2	40.4	17.8	0.0035	1.03	107	Buckled							
			A3	43.7	28.7	0.0037	1.09	162	Buckled							
		Design B $\varepsilon_D = 0.0080$	B1	40.6	22.1	0.0072	0.90	402	Ultimate							
			B2	40.6	22.1	0.0080	1.00	443	Ultimate							
			B3	40.6	22.1	0.0082	1.03	453	Ultimate							
			B4	40.6	22.1	0.0082	1.03	453	Ultimate							
	1.27 cm dia. cutout		B5	40.6	36.8									0.0058	0.73	496
Impact Damage Tests	Damage in High Axial Stiffness Region	Low Axial Load	A4	43.7	28.7	0.0000	0	0		53.9		0	Width of hat base by 6.4 cm long	0.0036	1.05	166
			A5	43.7	40.1	0.0000	0	0		51.5		0	Width of hat cap by 3.6 cm long	0.0034	1.00	197
			B6	40.6	36.8	0.0003	0.04	22.2		50.6		22.2	2.5 cm wide by 3.8 cm long	0.0043	0.54	374
		High Axial Load	A3 ‡	43.7	28.7	0.0034	1.00	148		50.9		129	14.0 cm by 14.0 cm	0.0037	1.09	140
			B7	40.6	36.8	0.0030	0.38	258		53.3		229	No data available	0.0046	0.58	345
			B8	40.6	36.8	0.0040	0.50	351		57.9		Catastrophic Failure on Impact				
	Damage in Low Axial Stiffness Region		B9 ‡	40.6	36.8	0.0041	0.51	347		52.4		347	2.8 cm diameter circle width 5.1 to 6.4 cm spike at 45°			
						0.0055	0.69	469		50.9		467		0.0062	0.78	534 †

* Estimate based on ultrasonic test
† Loading stopped, did not fail
‡ Specimen used for multiple tests

ε_a = Applied axial strain
ε_D = Design axial strain

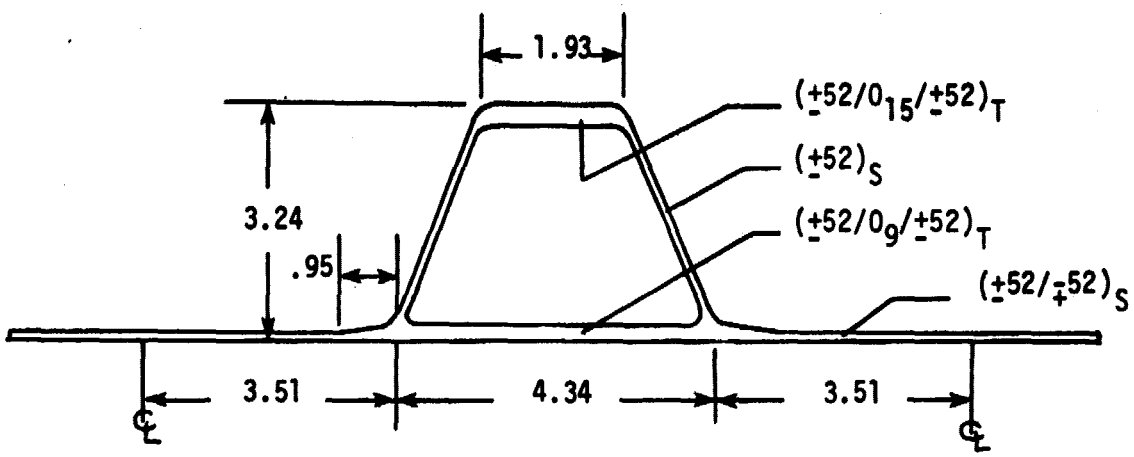

(a) Design A - Axial strain equals 0.0034 at applied design load of 0.53 MN/m. Axial stiffness of typical repeating element is 16.5 MN.

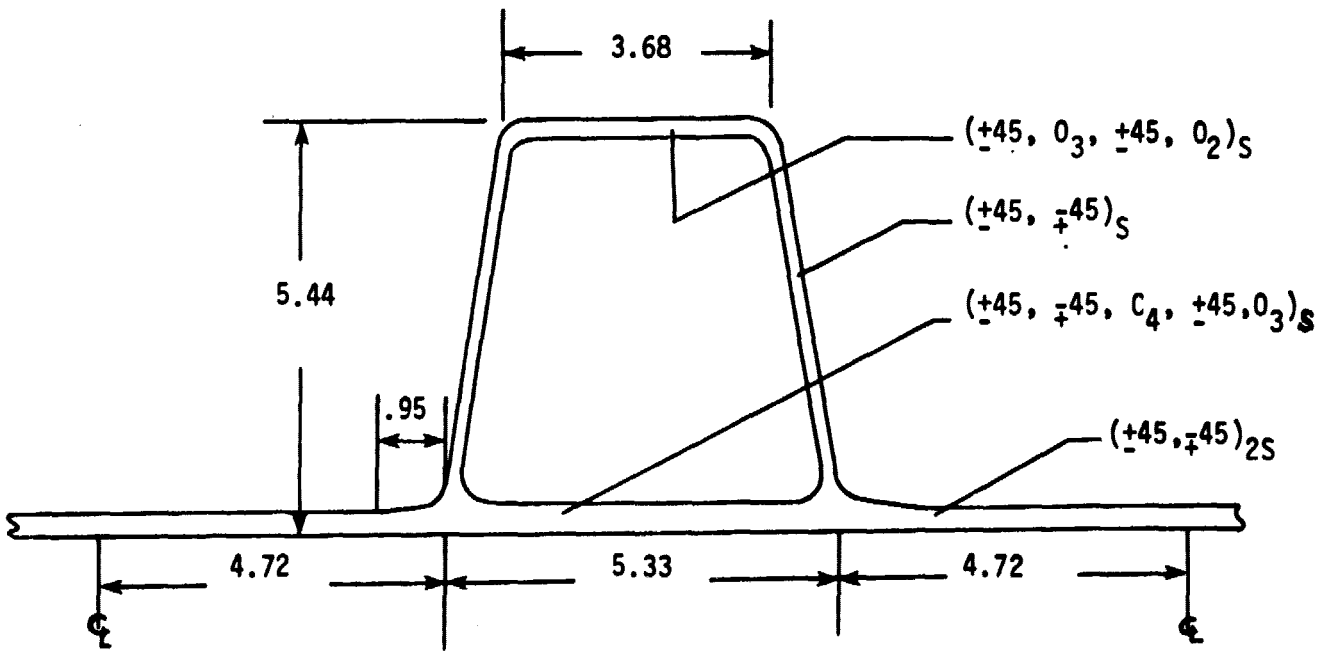

(b) Design B - Axial strain equals 0.0080 at applied design load of 1.58 MN/m. Axial stiffness of typical repeating element is 31.7 MN.

Figure 1.- Design details of typical stiffener cross-sections (dimensions in centimeters).

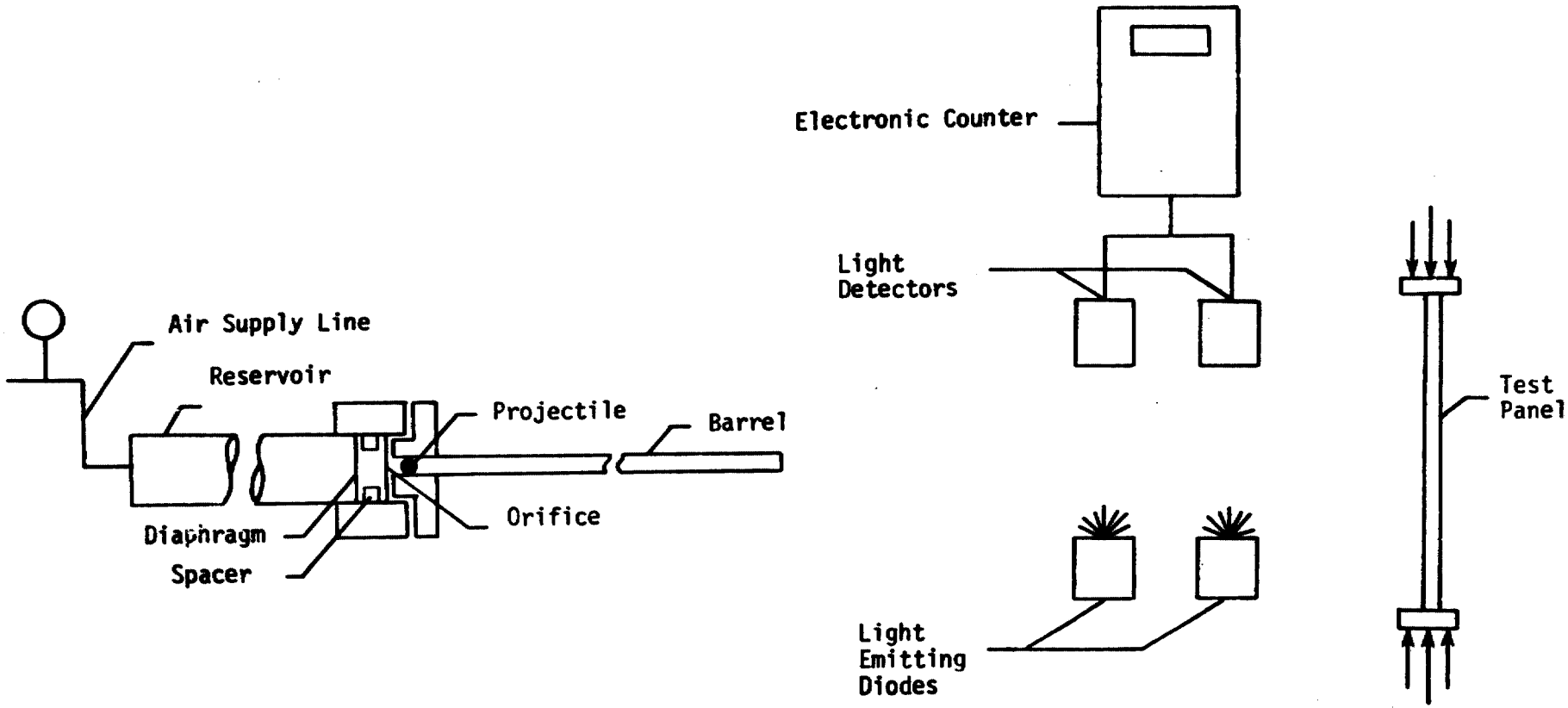

Figure 2.- Schematic of air gun and velocity detector.

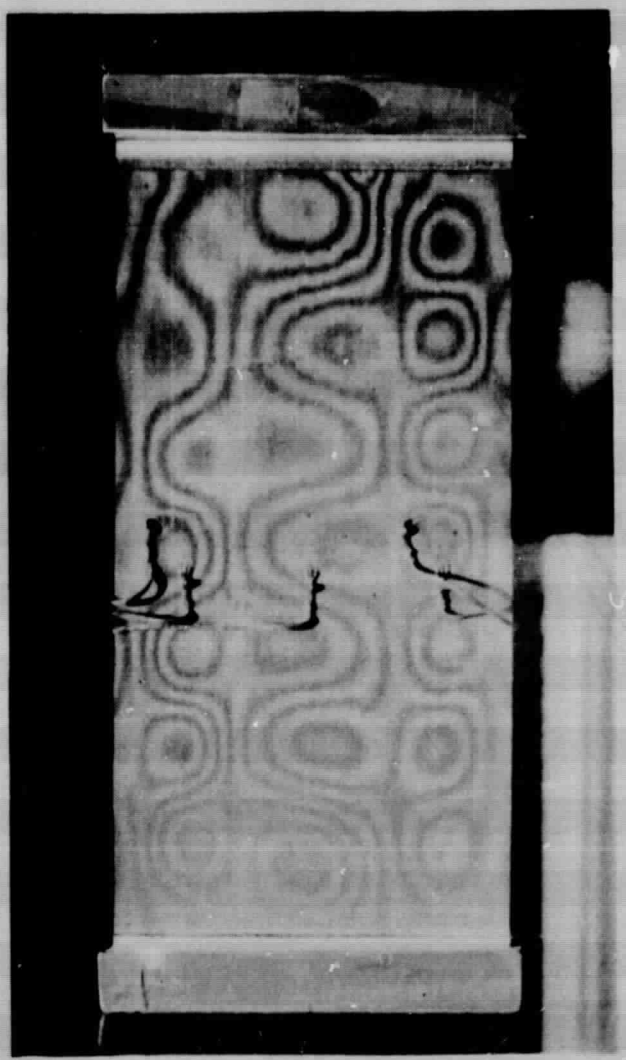

a) Panel A1 designed for strain of 0.0034 loaded to an applied axial strain of 0.0036.

b) Panel B2 designed for strain of 0.0080 loaded to an applied axial strain of 0.0079.

Figure 3.- Photographs of the moire' fringe patterns for typical undamaged panels during compression tests.

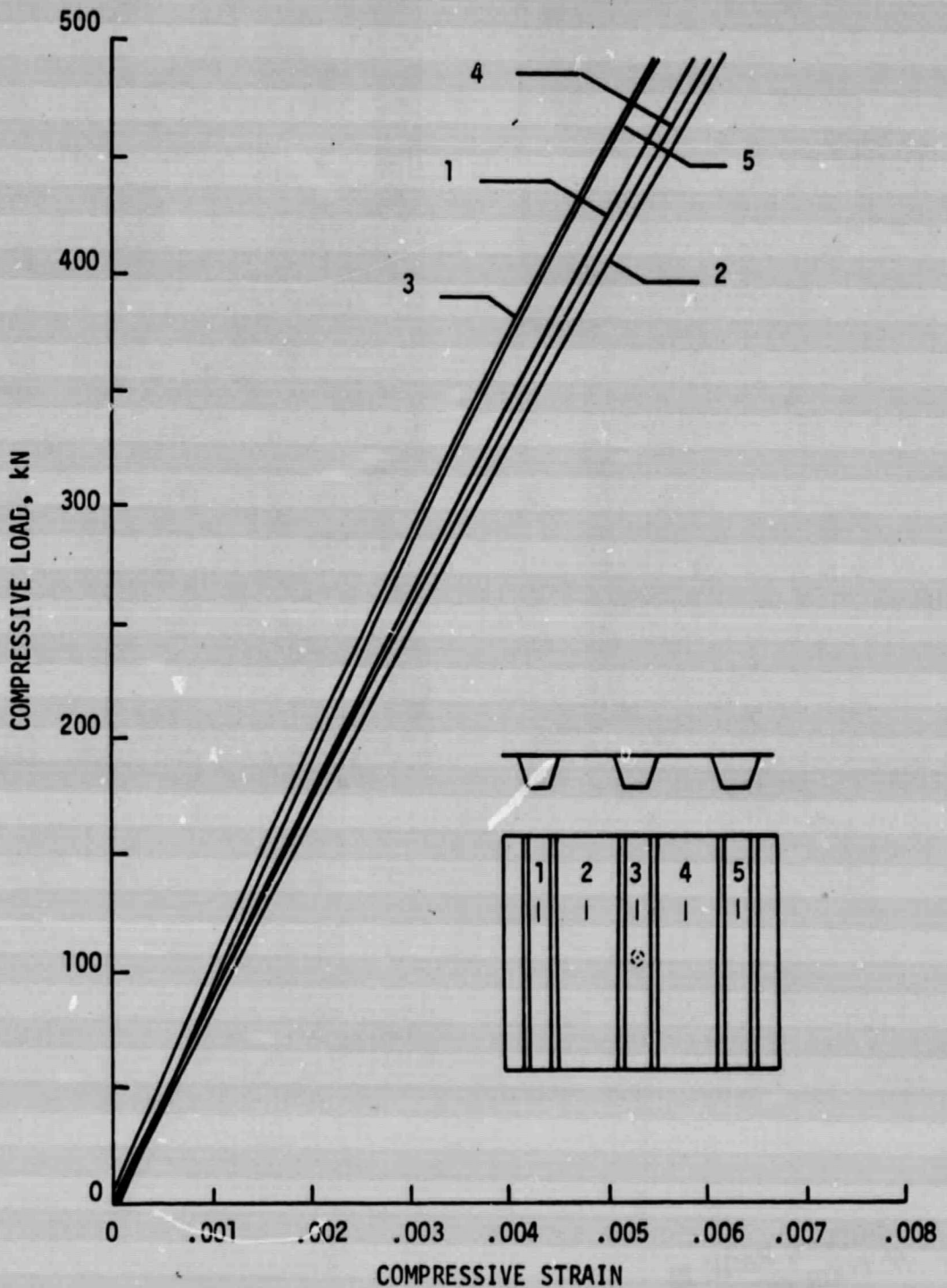

Figure 4.- Compression load-strain curves at 5 locations across Panel B5 which has a 1.27 cm diameter cutout in the high axial stiffness region of the center stiffener.

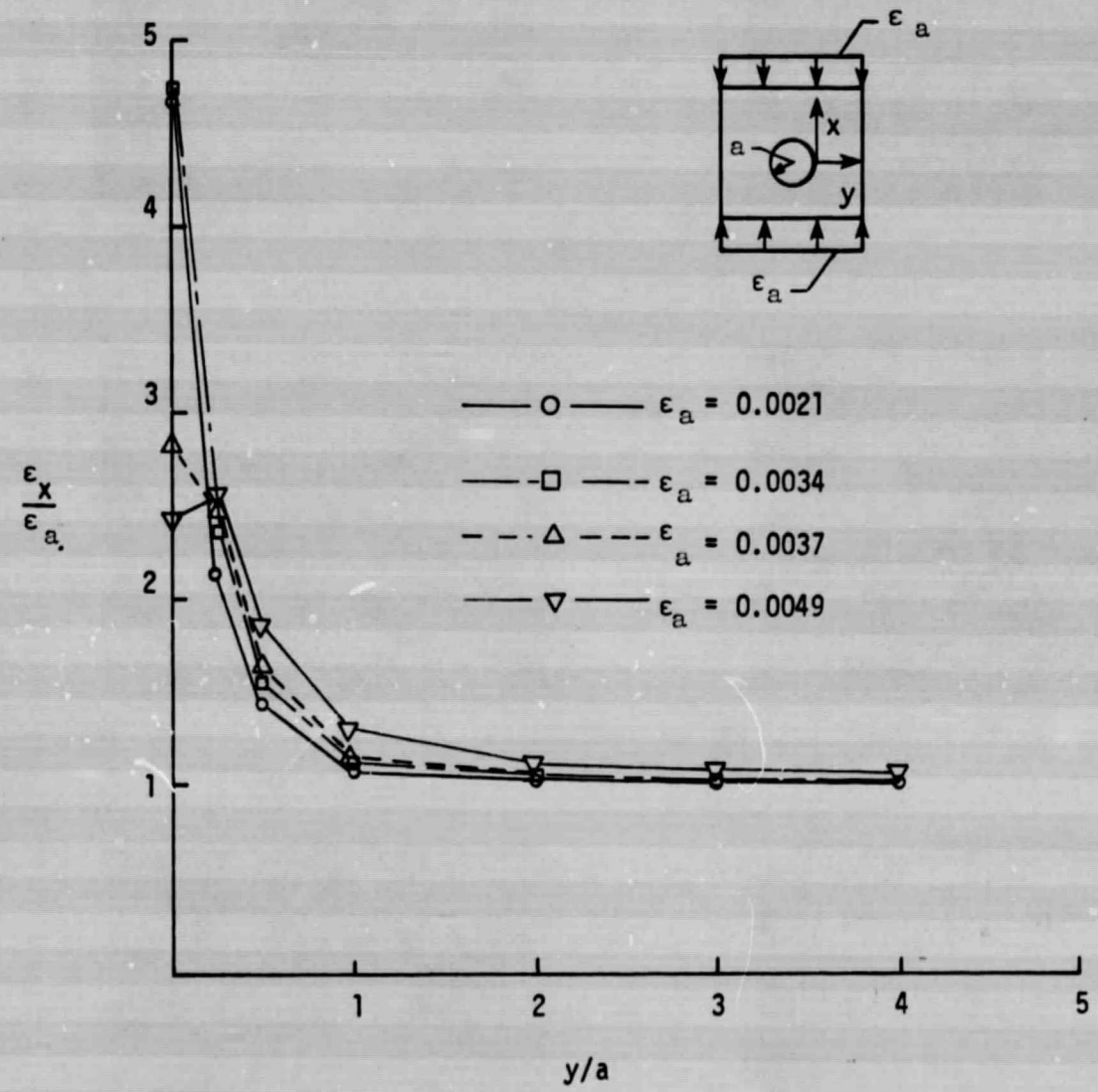

Figure 5.- Strain measured in the vicinity of the 1.27 cm diameter cutout on Panel B5. ε_x denotes measured strain at indicated location at an applied axial panel strain of ε_a.

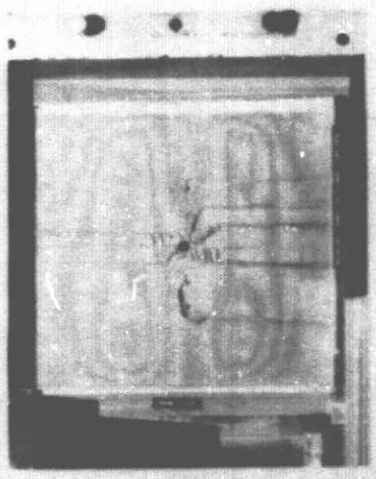

(a) ε_a = 0.0048

(b) ε_a = 0.0048

(c) ε_a = 0.0050

(d) ε_a = 0.0055

(e) ε_a = 0.0057

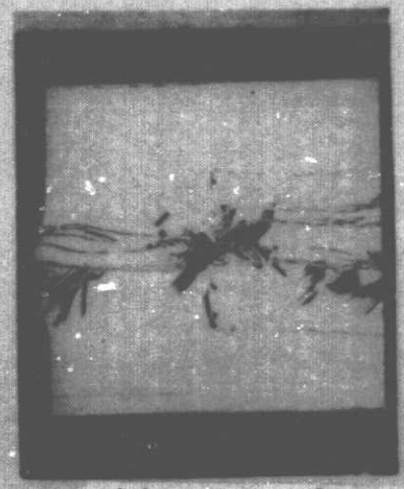

(f) ε_a = 0.0058

Figure 6.- Photographs of moire' fringe patterns of Panel B5 at several values of applied axial strain, ε_a.

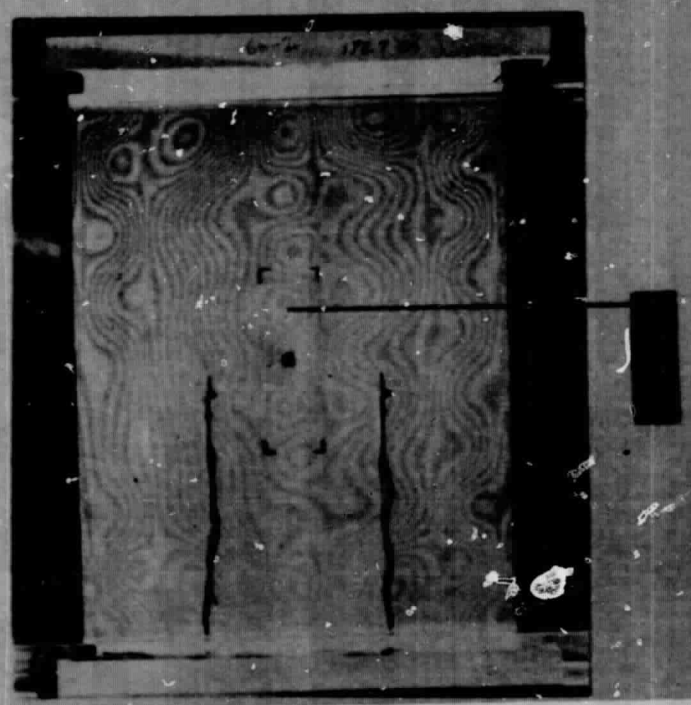

a) Photograph of moire' fringe pattern of buckled panel at an applied axial strain of 0.0035. Insert shows region of subsurface damage.

b) Test panel after failure at applied strain of 0.0036.

Figure 7.- Panel A4 after impact in the high axial stiffness region while at zero applied axial strain.

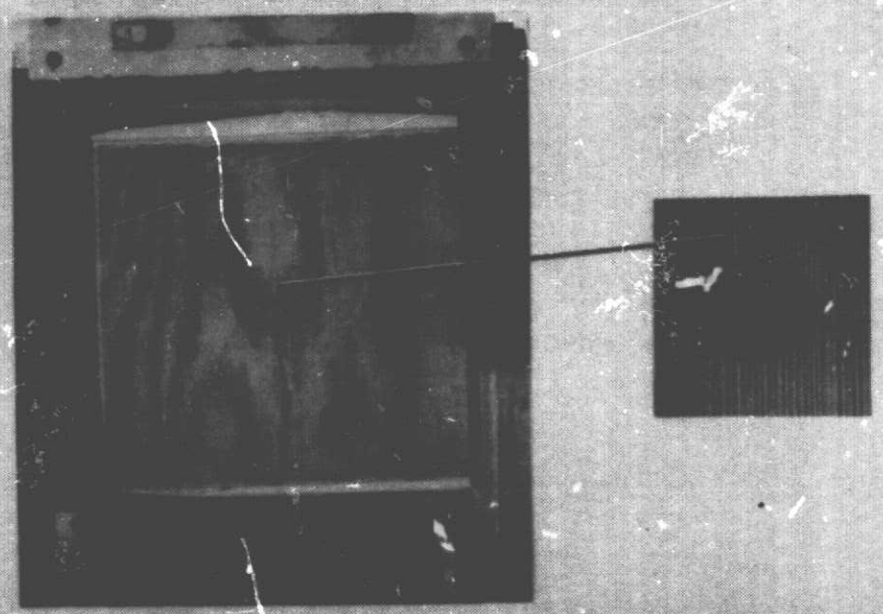

a) Photograph of moire' fringe pattern at applied axial strain of 0.0041 showing the development of a fringe pattern near the point of impact. Insert shows region typical of subsurface damage in a similar test panel.

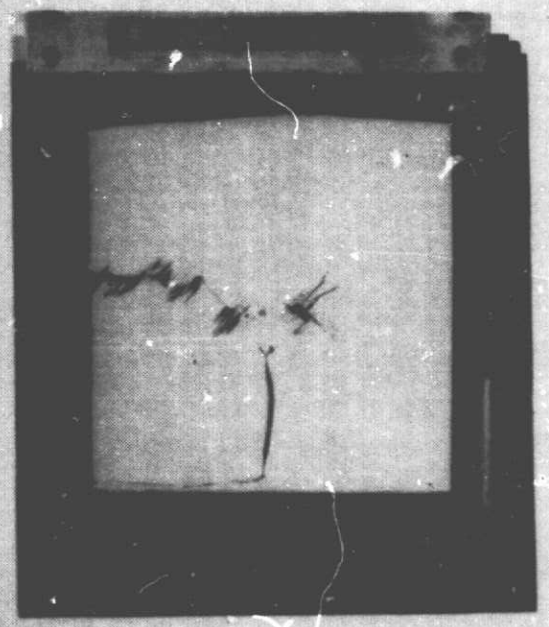

b) Test panel after failure at applied strain of 0.0043.

Figure 8.- Panel B6 after impact in the high axial stiffness region while at an applied strain of 0.0003.

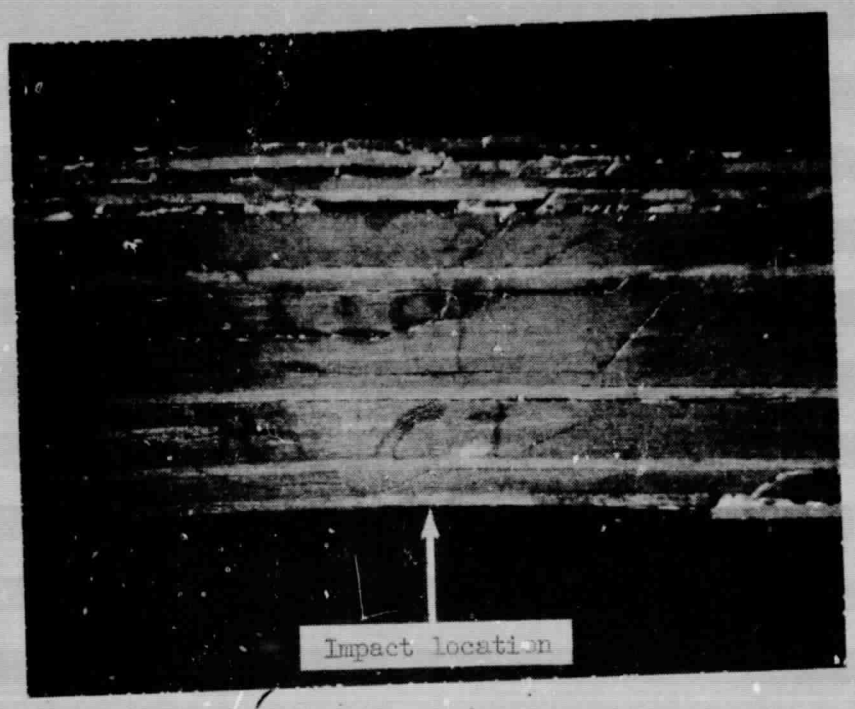

Figure 9.- Photomicrograph of the cross-section of the high axial stiffness region of a panel similar to B6 after being subjected to impact damage at zero applied axial strain.

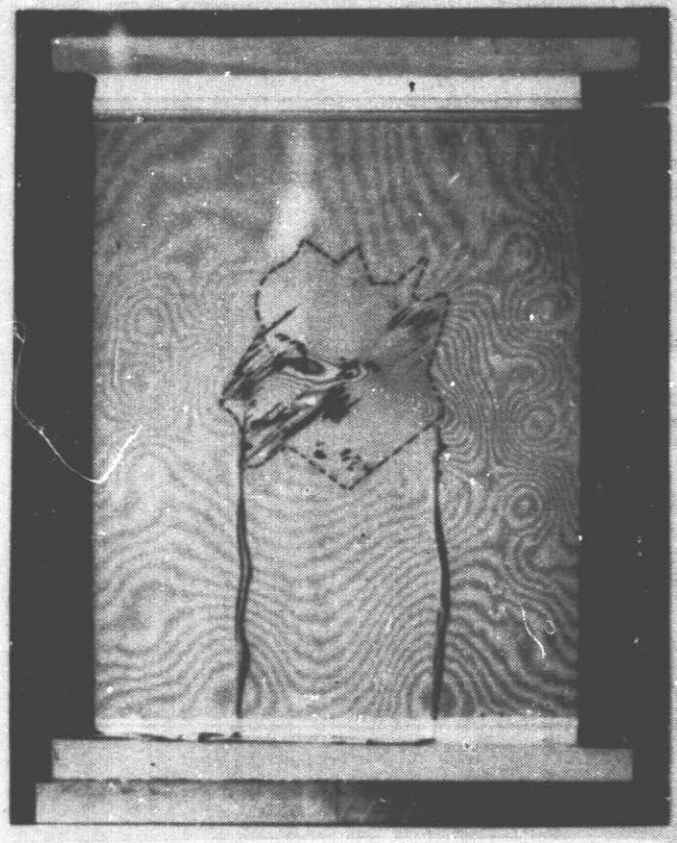

a) Photograph of moire' fringe pattern of buckled panel at an applied axial strain of 0.0031.

b) Test panel after failure at applied strain of 0.0037.

Figure 10.- Panel A3 after impact in the high axial stiffness region while at an applied strain of 0.0034.

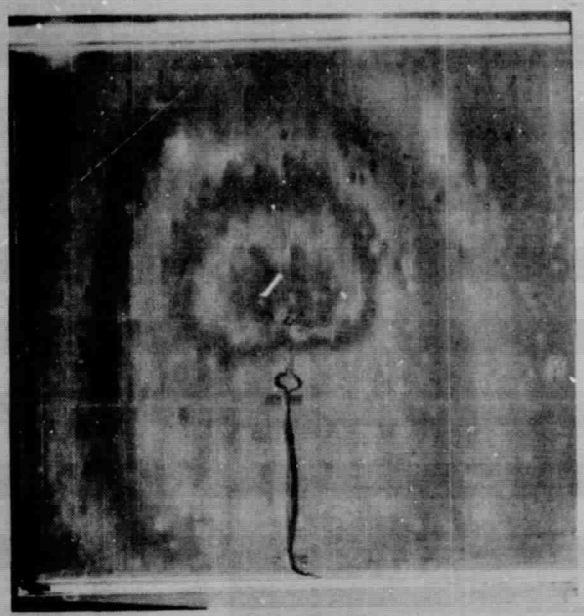

a) Panel with zero applied strain.

b) Panel loaded to applied strain of 0.0021.

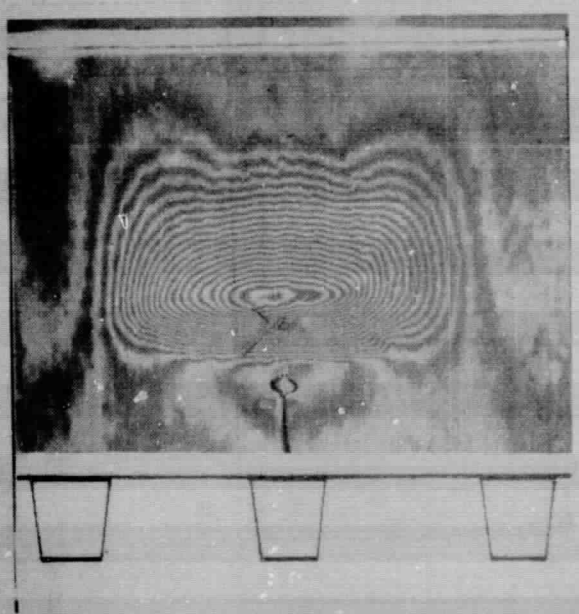

c) Panel loaded to applied strain of 0.0043.

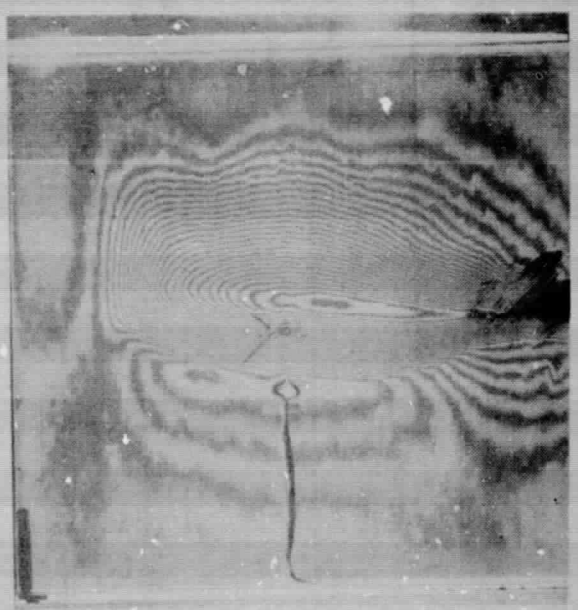

d) Panel after failure at applied strain of 0.0046.

Figure 11.- Panel B7 after impact in the high axial stiffness region while at an applied strain of 0.0030.

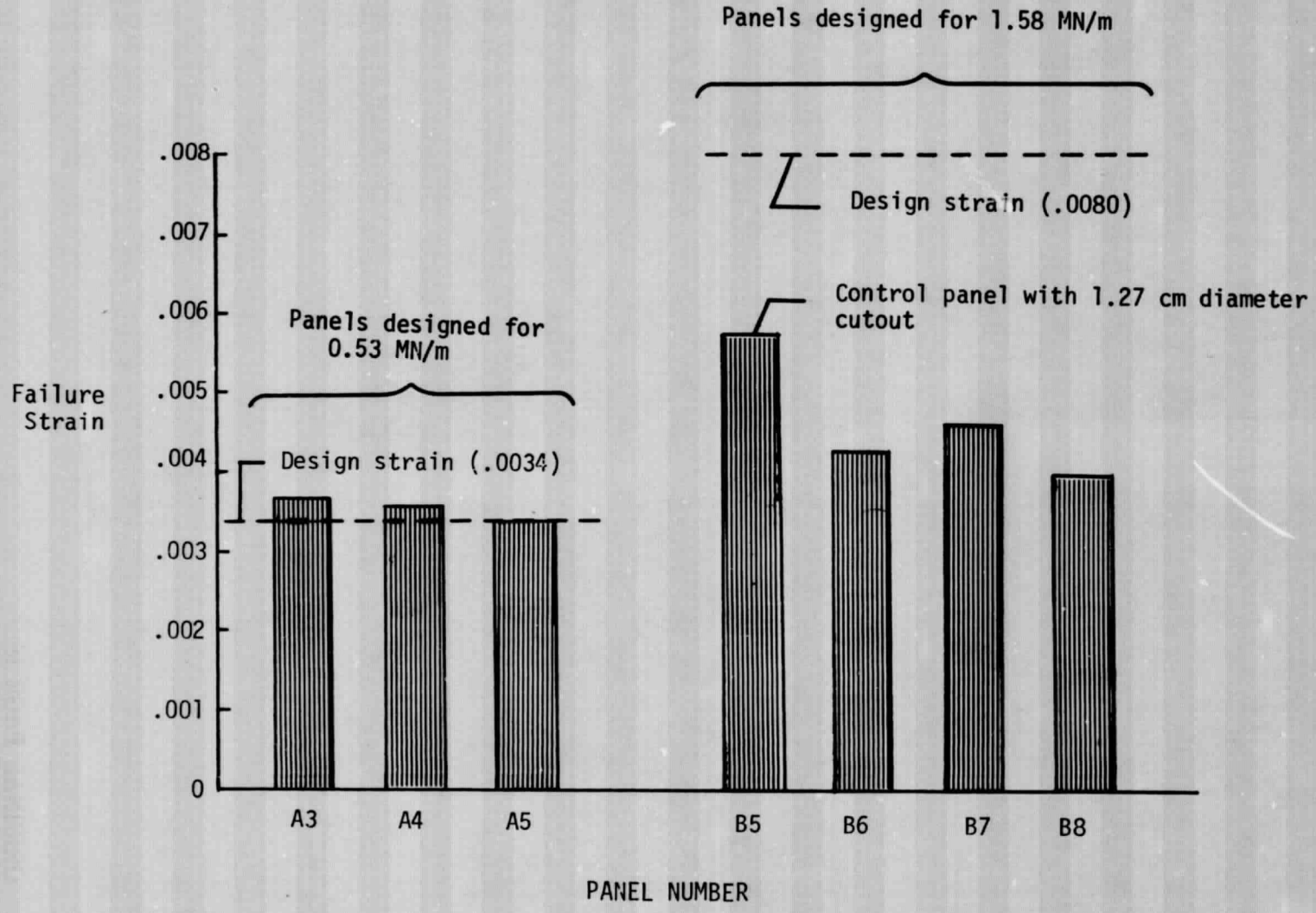

Figure 12.- Comparison of failure strains for panels damaged in high axial stiffness region.

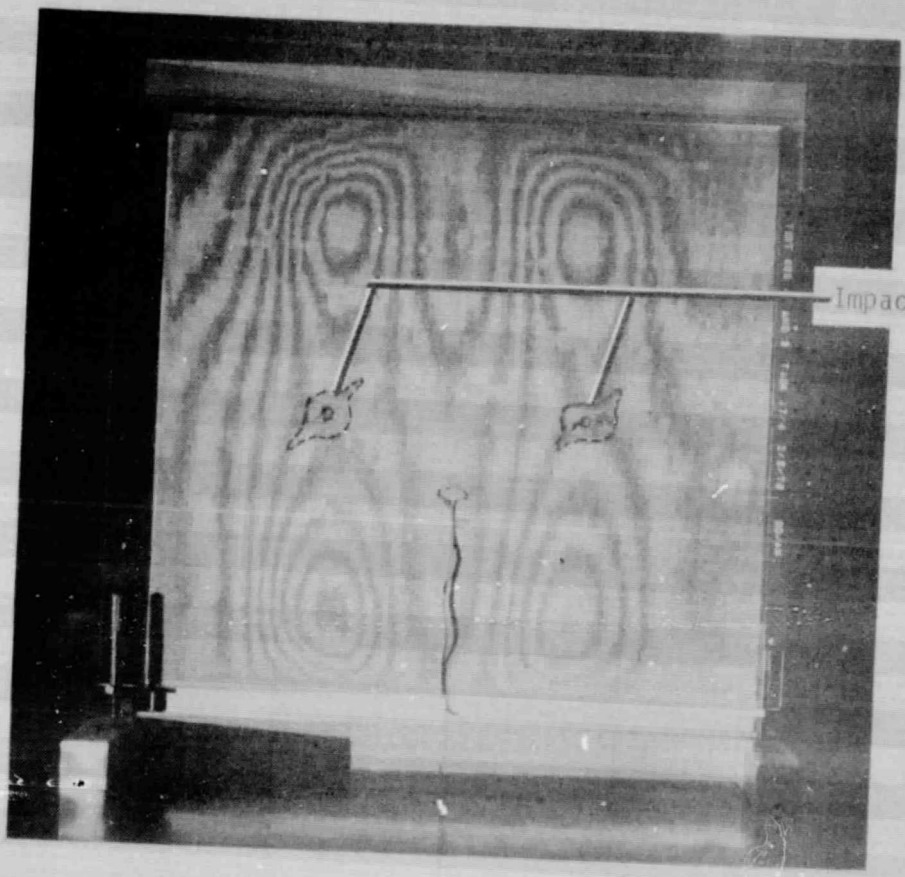

Figure 13.- Photographs of the moire' fringe pattern for Panel B9 at an applied axial strain of 0.0002 with impact damage at two locations in the low axial stiffness region.